

Coexistence of non-trivial van der Waals magnetic orders enable field-free spin-orbit torque switching at room temperature

Bing Zhao¹, Lakhan Bainsla^{1,2}, Roselle Ngalyo¹, Peter Svedlindh³, Saroj P. Dash^{1,4*}

¹*Department of Microtechnology and Nanoscience, Chalmers University of Technology, SE-41296, Göteborg, Sweden.*

²*Department of Physics, Indian Institute of Technology Ropar, Roopnagar 140001, India.*

³*Department of Materials Science and Engineering, Uppsala University, Uppsala, SE-751 03 Sweden.*

⁴*Graphene Center, Chalmers University of Technology, Göteborg, SE-41296 Sweden.*

Abstract

The discovery of van der Waals (vdW) materials exhibiting non-trivial and tunable magnetic interactions at room temperature can give rise to exotic magnetic states, which are not readily attainable with conventional materials. Such vdW magnets can provide a unique platform for studying new magnetic phenomena and realising magnetization dynamics for energy-efficient and non-volatile spintronic memory and logic technologies. Recent developments in vdW magnets have revealed their potential to enable spin-orbit torque (SOT) induced magnetization dynamics. However, the deterministic and field-free SOT switching of vdW magnets at room temperature has been lacking, prohibiting their potential applications. Here, we demonstrate magnetic field-free and deterministic SOT switching of a vdW magnet ($(\text{Co}_{0.5}\text{Fe}_{0.5})_5\text{GeTe}_2$ (CFGT)) at room temperature, capitalizing on its non-trivial intrinsic magnetic ordering. We discover a coexistence of ferromagnetic and antiferromagnetic orders in CFGT at room temperature, inducing an intrinsic exchange bias and canted perpendicular magnetism. The resulting canted perpendicular magnetization of CFGT introduces symmetry breaking, facilitating successful magnetic field-free magnetization switching in the CFGT/Pt heterostructure devices. Furthermore, the SOT-induced magnetization dynamics and their efficiency are evaluated using 2nd harmonic Hall measurements. This advancement opens new avenues for investigating tunable magnetic phenomena in vdW material heterostructures and realizing field-free SOT-based spintronic technologies.

Keywords: $(\text{Co}_{0.5}\text{Fe}_{0.5})_5\text{GeTe}_2$, 2D magnets, 2D materials, Room temperature, Spin-orbit torque, ferromagnet, anti-ferromagnet, Exchange bias, canted magnetism, Field-free magnetization switching.

Corresponding author: saroj.dash@chalmers.se

Introduction

The next generation of memory, logic, communication, and beyond von Neumann computing architecture are expected to benefit from the use of energy-efficient and non-volatile spintronic technologies^{1,2}. Recently, the spin-orbit torque (SOT) phenomenon, which utilizes the spin-orbit interaction in materials and their hybrid structures with magnets, has emerged as an efficient method to control the magnetization in spintronic devices³⁻⁵. The control of magnetization by SOT is an attractive alternative to spin-transfer torque (STT) used in magnetic random access memory, spin-logic and spin nano-oscillator technologies, as SOT-based devices are more energy efficient, ultrafast, and provide increased data density with high endurance⁵. However, for the commercial success of SOT-based technology, it is required to enhance the SOT efficiency, achieve magnetic field-free magnetization switching, and discover new materials and methods to control the device parameters^{2,6-9}.

Recently discovered two-dimensional van der Waals (vdW) magnetic materials have significant potential for spintronic devices because of their low dimensionality, tunable magnetic anisotropy, strong proximity-induced interactions, and potential for voltage-controlled magnetism^{2,10-14}. Recent advancements in vdW magnets include the SOT-induced magnetization switching of Fe_3GeTe_2 with perpendicular magnetic anisotropy (PMA) in heterostructures with different spin-orbit materials (SOMs) at cryogenic temperatures^{6,15-18}. However, devices including conventional SOMs such as Pt require assistance from an external in-plane magnetic field to break the symmetry¹⁹ or need materials with low crystal symmetry such as WTe_2 with an out-of-plane SOT component^{6,20} to deterministically switch the magnetization of Fe_3GeTe_2 without an external field. Unfortunately, due to the low Curie temperature (T_c) of Fe_3GeTe_2 , the operation of these SOT devices is limited to cryogenic temperature and the SOT efficiency of WTe_2 is much smaller than Pt^{6,20}.

Being able to control properties of vdW magnets, such as the interlayer exchange coupling inherent to vdW magnets and the canted state of magnetization, could also help to achieve field-free SOT switching^{7-9,21}. To address this, vdW magnets can be tailored to have unique non-trivial spin ordering due to exchange coupling depending on atomic position, stacking, and intra- and interlayer magnetic interactions²²⁻²⁴. Specifically, the possibility of taking advantage of coexisting ferromagnetic (FM) and antiferromagnetic (AFM) phases in a single vdW material to achieve field-free SOT switching remains unexplored.

Here, we demonstrate deterministic SOT-induced magnetization switching of the vdW magnet $(\text{Co}_{0.5}\text{Fe}_{0.5})_5\text{GeTe}_2$ (CFGTe) at room temperature without using any external magnetic field. This has been possible due to the non-trivial spin ordering with the coexistence of FM and AFM ordering in CFGTe accompanied by a pronounced exchange bias effect and canted magnetization that persist above room

temperature, which is not readily attainable with conventional materials. To gain deeper insights into the magnetic properties of CFGT and their correlation with the SOT switching behavior in CFGT/Pt heterostructure Hall-bar devices, we employed the anomalous Hall effect, current-induced magnetization switching, and 2nd harmonic Hall measurements. Our findings reveal that the field-free SOT-induced magnetization switching in CFGT arises from its canted magnetization, which can be induced by the intrinsic exchange bias within the CFGT magnet. This addresses critical aspects in the advancement of vdW-magnet-based spintronic technologies.

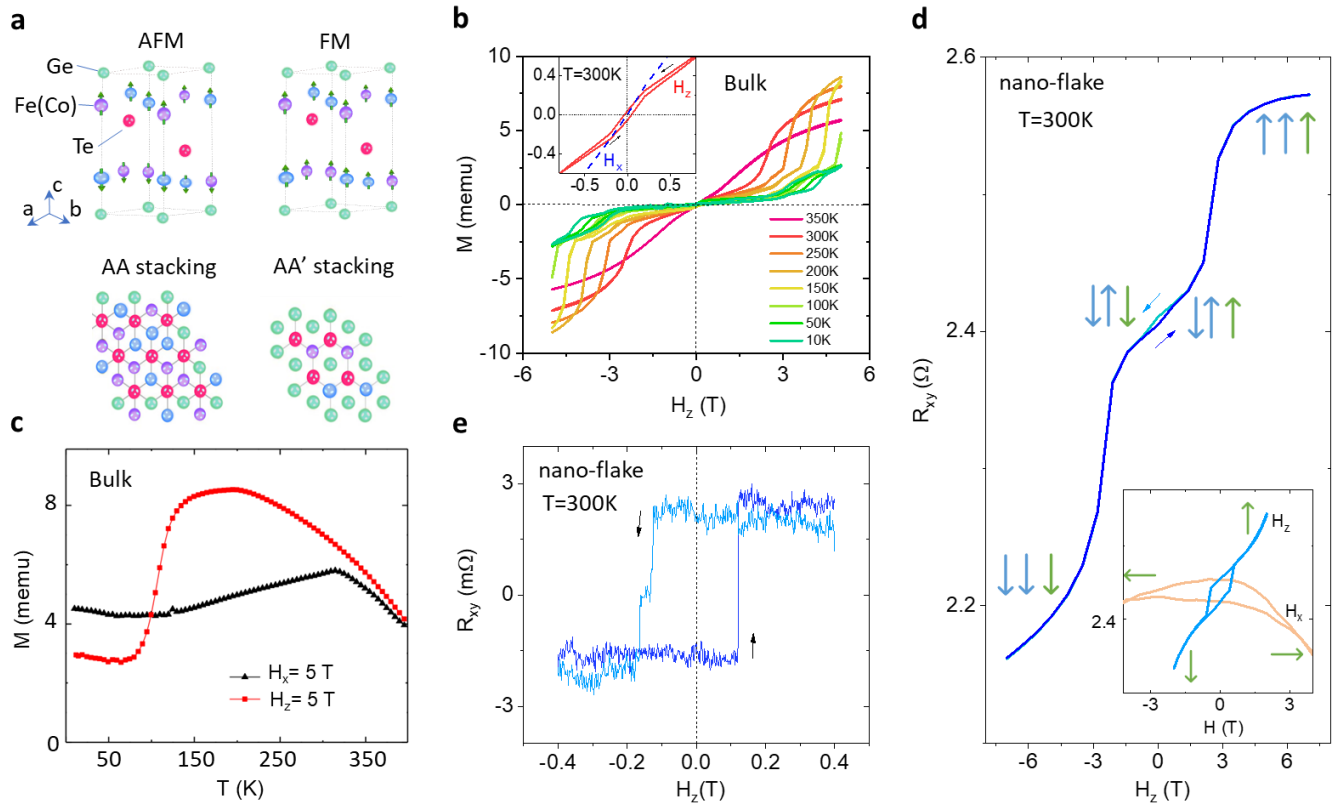


Figure 1. Coexistence of ferro- and antiferro- magnetism in $(\text{Co}_{0.5}\text{Fe}_{0.5})_5\text{GeTe}_2$ above room temperature. **a.** Schematic of the crystal structure of CFGT with AA (AFM) and AA' (FM) stacking order, respectively. The arrows are the atomic magnetic moment in Fe(Co)-site. **b.** The out-of-plane magnetic field H_z dependence of the magnetization of bulk CFGT measured with SQUID. The inset is the zoom-in of the data at 300 K, the dashed curve corresponds to the magnetization measured using an in-plane magnetic field H_x . **c.** Temperature dependence of the magnetization measured with a fixed in-plane (H_x) and out-of-plane (H_z) magnetic field of 5T. **d.** Transversal Hall resistance (AHE) $R_{xy}=V_{xy}/I$ of a CFGT nanoflake as a function of the out-of-plane field (H_z) at 300 K in the field range of ± 7 Tesla. The (blue/green) arrows show the AFM and FM magnetic spin configurations. Inset shows R_{xy} versus H_x and H_z in the field range ± 4 Tesla. **e.** AHE signal at 300 K in a small field range after subtraction of a linear background.

Results and Discussion

Coexistence of ferromagnetic and antiferromagnetic orders in CFGT at room temperature: Exchange bias and canted magnetism

The motivation behind using the vdW magnet CFGT is its beyond room temperature magnetic order and tunable magnetic properties depending on atomic positions, stacking, and intra- and interlayer magnetic interactions^{22–24}. CFGT with the wurtzite crystal structure belongs to the $P6_3mc$ space group and C_{6v} point group²⁵. By substituting around 50% of the Fe atoms with Co, crystals of CFGT alloy were synthesized (from Hq Graphene), where AA' (FM intralayer coupling) and AA (AFM interlayer coupling) atomic crystal structures possibly coexist (Fig. 1a)^{23,25}. Theoretical calculations²⁴ predicted that it is the combination of high Co content and the concomitant change to primitive layer stacking that produces different non-trivial magnetic orders. The intralayer coupling is dominantly ferromagnetic, while the unique primitive unit cell contains the possibility of AFM interlayer coupling, which makes such a vdW magnet particularly interesting and elusive. The coexistence of FM and AFM order provides an added advantage of an exchange bias effect in a single vdW magnetic material and offers a unique platform for the possible realization of field-free SOT magnetization switching.

Out-of-plane magnetization measurements on bulk CFGT samples at different temperatures using a superconducting quantum interference device (SQUID) show a characteristic magnetic field-induced spin-flop transition between antiferromagnetically and ferromagnetically aligned layers of CFGT at large field (Fig. 1b)^{26,27}. Observing a hysteresis loop in the low field range at 300 K, suggests the coexistence of both FM and AFM phases (Fig. 1b, inset). The temperature-dependent SQUID measurements with fixed in-plane and out-of-plane fields further confirm the magnetic behaviour of CFGT beyond 350 K, with an anomalous behavior observed at low temperatures, indicating a possible phase transition²⁸ (Fig. 1c).

To investigate the magnetic properties of thin CFGT flakes (30–50 nm), magnetotransport measurements using the anomalous Hall effect (AHE) were conducted on nanofabricated Hall-bar devices (see Methods section Supplementary Fig. S1 for details). The AHE measurements (Hall resistance R_{xy} as a function of the out-of-plane magnetic field H_z) of CFGT thin flakes at 300 K revealed the coexistence of FM and AFM below the spin-flop transition, as shown in Fig. 1d. Along with the observed spin-flop transitions at higher fields, a distinct hysteresis loop appeared in the low field range indicating the presence of a ferromagnetic component of the magnetization. A further detailed measurement with both in-plane and out-of-plane fields (inset of Fig. 1d) and low field measurements (Fig. 1e) suggested an out-of-plane magnetism in CFGT with finite remanence and coercivity at room temperature. Upon removal of the linear background, the

square loop-like AHE signal confirmed the ferromagnetism and most importantly with an exchange bias effect²⁹, which is manifested as a horizontal shift in a magnetic hysteresis loop due to the coexistence of intrinsic FM and AFM phases in CFGT.

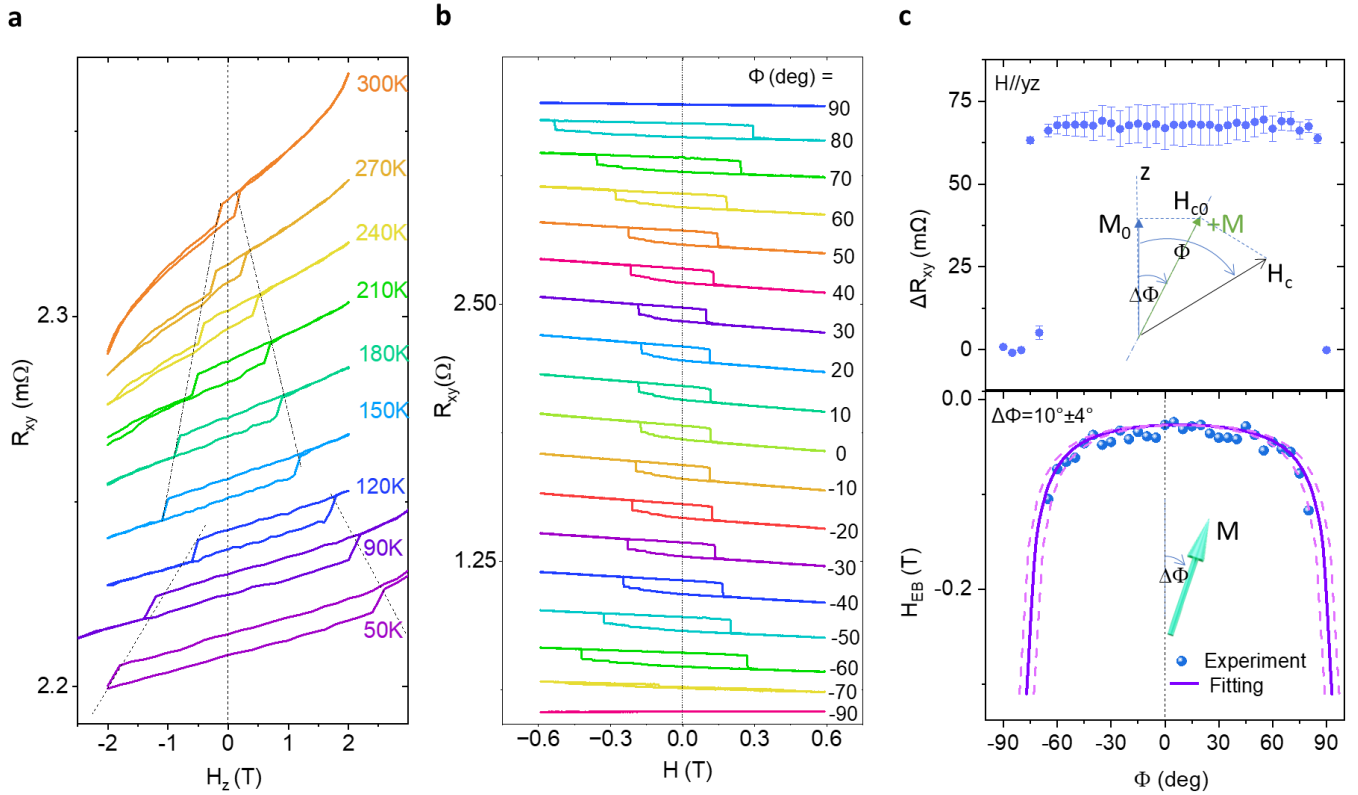


Figure 2. Exchange bias and canted perpendicular magnetic anisotropy of CFGT. **a.** Transversal Hall resistance R_{xy} with out-of-plane field H_z at different temperatures in low field range. The dashed lines are the guide to the eye. **b.** AHE signals R_{xy} with different out-of-plane angles Φ of the magnetic field at 300 K. **c.** The extracted magnitude of the AHE signal ΔR_{xy} and exchange bias field H_{EB} as a function of the out-of-plane angle. The purple curve in the bottom panel is a fit (see main text for details) with uncertainty represented by dashed curves. The insets show the schematics of the magnetization M with a canting angle $\Delta\Phi$ and its relation with the external field H_c .

Figures 2a illustrate the evolution of the AHE signal of CFGT with temperature in the range of 50-300 K, where apparent hysteresis is observed in a smaller magnetic field range. At lower temperatures, the coercivity increases and the exchange bias effect become more prominent. The exchange bias effect is larger around 120 K, consistent with a magnetic phase transition observed in SQUID measurements (see Supplementary Fig. S2). Due to the presence of both FM and AFM properties in CFGT flakes, there is a possibility that its magnetic anisotropy may be significantly impacted. To examine this, we conducted an angle-dependence study of the AHE on the CFGT/Pt Hall-bar device at room temperature (Fig. 2b). The AHE signal with exchange bias effect can be observed at all angles, except for the in-plane case where

the signal vanishes. The magnitude of the AHE signal remains constant up to higher angles, indicating a strong magnetic anisotropy and minimal rotation of the magnetization towards the field direction (Fig. 2c). The extracted exchange bias field $H_{EB}=(H_{C+}+H_{C-})/2$ at different angles are presented in Fig. 2c (bottom panel), where $H_{C\pm}$ are the switching fields in positive/negative directions. We consider $H_{C0\pm}$ to be the coercive fields required to switch $-(+)$ M to $+(-)$ M when the applied magnetic field is aligned with the easy axis of the magnetization. Further, assuming that the rotation of the magnetization is negligible when changing the applied field by an angle Φ , implies that the projection of the applied field on the easy axis of the magnetization must be equal to $H_{C0\pm}$ to switch the magnetization; $H_{C0\pm} = H_{C\pm} \cos(\Phi - \Delta\Phi)$, where $\Delta\Phi$ defines the easy axis of magnetization. The formulated relation between H_{EB} and the field rotation angle Φ is fitted to the angle-dependent results, indicating a magnetization canting angle $\Delta\Phi$ of ~ 10 degrees in CFGT (see details in Supplementary Note 1).

Room temperature field-free spin-orbit torque switching of CFGT/Pt heterostructure devices

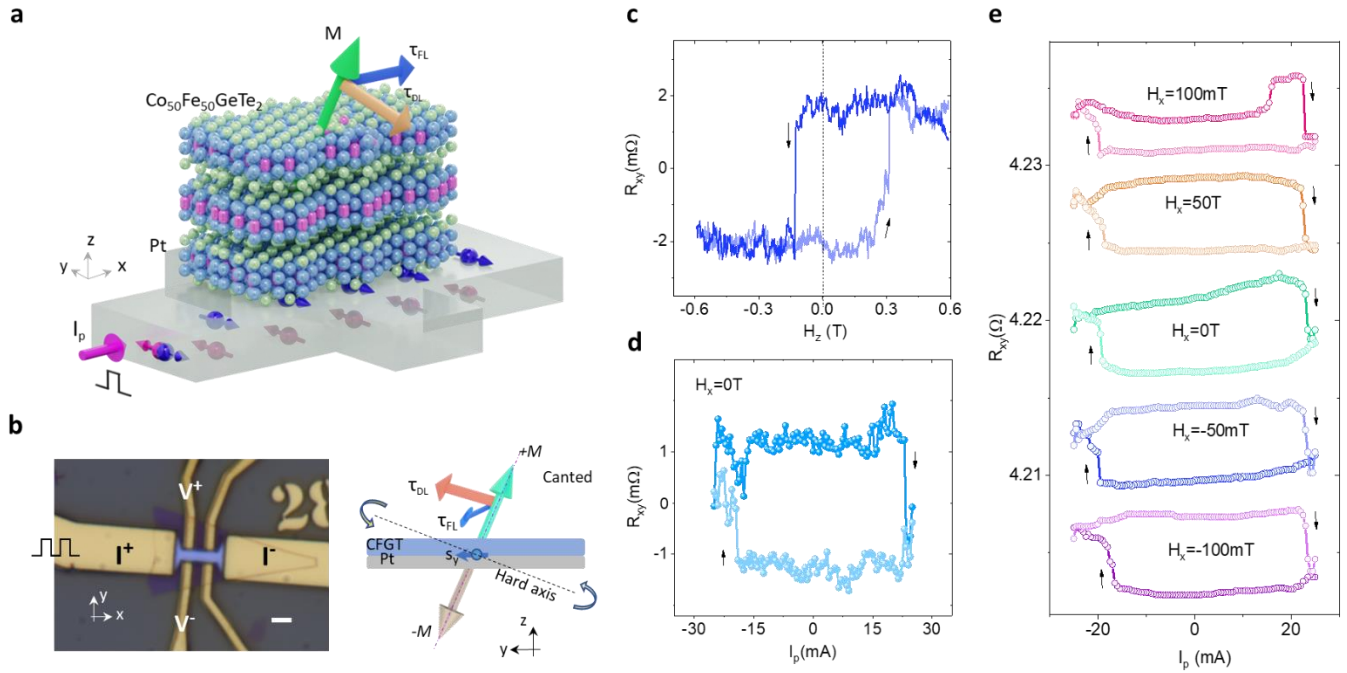


Figure 3. Field-free spin-orbit torque magnetization switching in CFGT/Pt heterostructure at room temperature. **a.** Schematics of CFGT/Pt van der Waals heterostructure used for spin-orbit torque (SOT) experiments. The pulsed charge current I_p applied to Pt generates a spin current J_s due to the spin Hall effect, creating a damping-like torque (τ_{DL}) and field-like torque (τ_{FL}) acting on the magnetization M of CFGT. **b.** Left panel: Optical microscope image of the CFGT/Pt heterostructure Hall-bar device with measurement geometry for AHE and SOT experiments in Dev 1. The scale bar is $2 \mu\text{m}$. Right panel: Schematic for SOT switching of CFGT with a canted magnetization M . The dashed lines indicate the canted easy axis and hard axis of magnetization in CFGT. The

arrows show the M switching direction. **c.** Pulsed write current I_p induced transverse Hall signal R_{xy} change due to SOT-induced magnetic switching without external magnetic field. **d,e.** The measured SOT magnetization switching signals with different in-plane fields H_x .

Spin-orbit torque (SOT) experiments provide a valuable platform for studying magnetization switching dynamics, and realization field-free switching of vdW FMs will offer practical spintronic device applications. To investigate the SOT-induced magnetization switching and dynamics in CFGT samples with intrinsic exchange bias and canted magnetization effects, CFGT/Pt heterostructure Hall bar devices were nanofabricated as shown in Figure 3a and 3b (see details in the Methods section). For an effective SOT magnetization switching, it is essential to have a large charge-spin conversion efficiency in Pt and high-quality CFGT/Pt interfaces for efficient transmission of spin current. In the SOT-induced magnetization switching experiment, a series of DC pulse currents applied along the x-direction through the spin-orbit material (Pt), generates a spin current along the z-axis with spin polarization s_y along the y-axis due to the spin Hall effect. The resulting spin current exerts SOTs in CFGT (field-like T_{FL} and damping-like T_{DL} torques), enabling the switching of magnetization M direction. Specifically, the field-like torque $T_{FL} \sim M \times s_y$, precesses M about the exchange field created by spin polarization, while the damping-like torque $T_{DL} \sim M \times (M \times s_y)$ rotates the magnetization M towards the direction of spin polarization s_y . Typically, damping-like torque determines the switching of the magnetization³⁰.

The AHE signal of the CFGT/Pt Hall device shows an out-of-plane field magnetization and the difference of the switching field for both field sweep directions suggests a strong exchange bias ($H_{EB} = 0.075$ T) in CFGT (Fig. 3c, the magnitude of exchange bias vary from device to device due to different flake thickness). As shown in Fig. 3d, we observed the SOT-induced magnetization switchings using a pulsed write current I_p with pulse time 100 μ s, followed by a small DC read current ($I_r \sim 50$ μ A) to probe the magnetization state $R_{xy} = V_{xy}/I_r$. As the signal R_{xy} is proportional to the out-of-plane magnetization M_z ⁴¹, the SOT signal shows current induced magnetization change between $+M_z$ and $-M_z$. The magnitude change of R_{xy} in the SOT signal is around 50% of the AHE signal with field sweep, which suggests around half of the CFGT magnetization is switched. Such partial switching could be due to some domain structure in the Hall-bar device and/or also short spin diffusion length in CFGT of \sim few nm, while the CFGT flakes are \sim 30 nm thick. Interestingly, we observe a deterministic SOT switching of CFGT without applying any magnetic field. This is in contrast to the conventional requirement of an in-plane magnetic field H_x to break the geometrical symmetry for a deterministic switching of the PMA magnetization. To verify the origin, we performed SOT measurements with different in-plane magnetic fields H_x (Fig. 3e). We found that the H_x field does not affect the SOT switching and the magnetization switching direction (chirality) remains the

same in this field range of +/-100 mT, suggesting that the external field does not play a significant role due to exchange bias effects, instead canted magnetization assist the deterministic switching of CFGT²¹.

Conventionally, chirality is determined by the external field, which favours opposite switching directions for the positive and negative in-plane magnetic fields¹⁹. If no external field is applied, the magnetization would be pulled to the in-plane orientation and broken into multiple domains, instead of the observed deterministic switching. However, in the canted magnetization scenario of CFGT sample (Fig. 3b), the symmetry is broken as the easy axis of the magnetization M is canted at an angle $\Delta\Phi$ with respect to the normal direction. The damping-like torque τ_{DL} can rotate the M anticlockwise over the hard axis towards another easy axis, while the other rotation direction is not possible. This also explains the unchanged chirality of SOT switching with the external field direction, which is similar to that observed in other canted magnets.²¹ Thermal fluctuations induced by pulse current can randomize the magnetic domain of CFGT and make switching behavior unstable¹⁶. This is not the case in our CFGT/Pt SOT device though the reduction of the SOT signal caused by the thermal fluctuations can not be ruled out¹⁸. We can also rule out thermally assisted switching if the device reaches above T_c , as this can result in undeterministic switching due to formation of multiple domains^{31,32}. Therefore, the observed deterministic and field-free switching of CFGT can be attributed dominant SOT contribution and the canted magnetization of CFGT.

Estimation of spin-orbit torque magnetization dynamics using harmonic Hall measurement in CFGT/Pt heterostructure devices

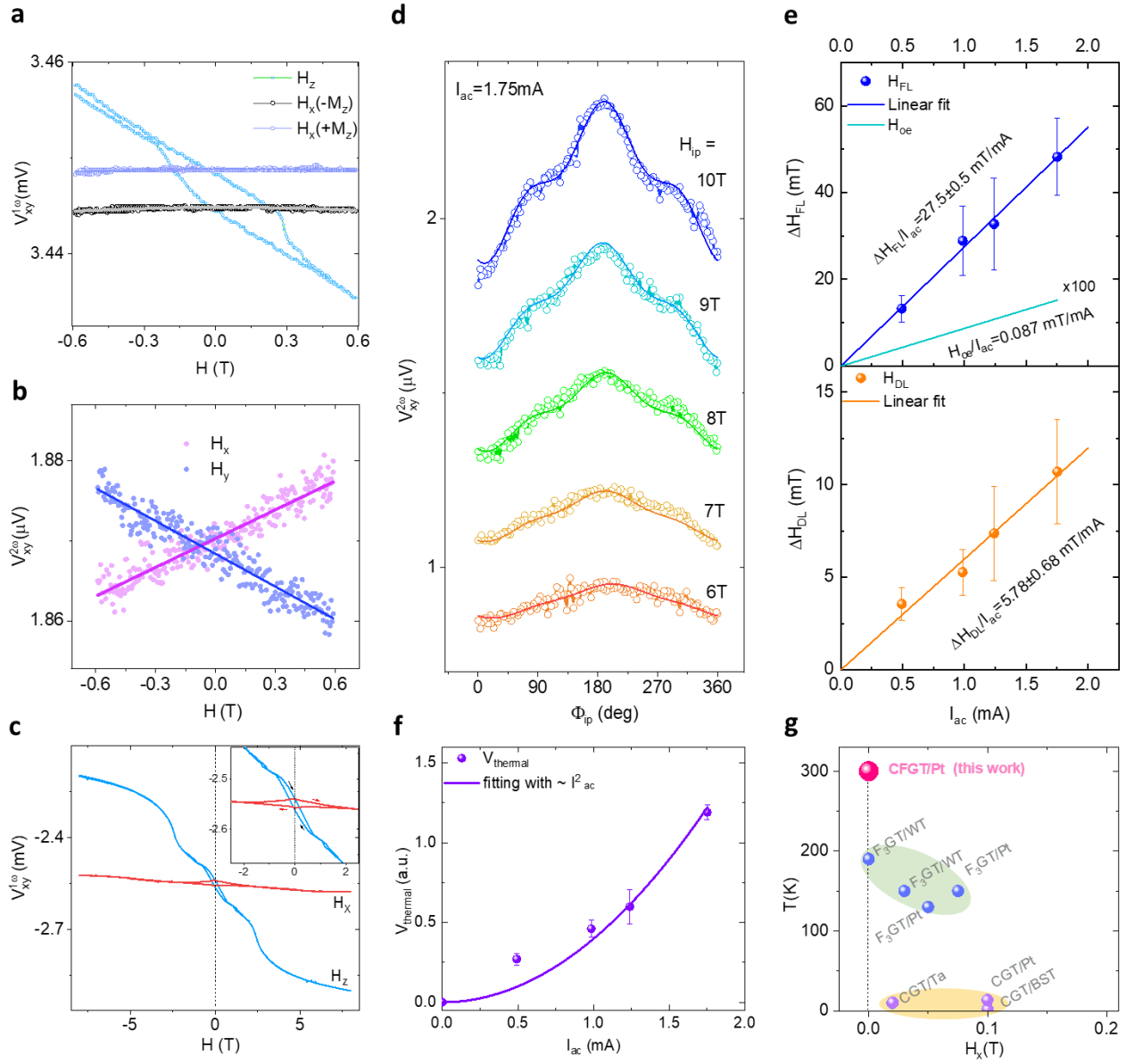


Figure 4. Harmonic Hall signals of the CFGT/Pt Hall-bar device at room temperature. **a.** 1st harmonic $V_{xy}^{1\omega}$ signals as a function of the out-of-plane field H_z and longitudinal in-plane field H_x sweeps with $\pm M_z$ magnetic states of CFGT. The solid lines are the fitting results of the longitudinal $V_{xy}^{1\omega}$ signals. **b.** Longitudinal (transversal) in-plane field $H_{x(y)}$ dependence of the 2nd harmonic signals $V_{xy}^{2\omega}$. The pink and blue lines are linear fits of the corresponding signals. All the harmonic measurements were performed with $\omega=213.14$ Hz and $I_{ac}=4.9$ mA at 300 K in Dev 2. **c.** Field dependence of the 1st harmonic $V_{xy}^{1\omega}$ signals with field directions indicated (H_z and H_x). The inset is the zoom-in around 0 T. **d.** In-plane angle dependence of the 2nd Harmonic signal at $I_{ac}=1.75$ mA with in-plane field H_{ip} . **e, f.** Extracted current dependence of the field-like effective field ΔH_{FL} , Oersted field H_{Oe} , damping-like effective field ΔH_{DL} , and thermal contribution in Dev 3. **g.** Benchmark plot showing the state-of-the-art of the vdW magnets based SOT devices, considering working temperature vs. in-plane assistant magnetic field H_x . Benchmarking our work with state of the art results using vdW magnet based SOT devices of Fe_3GeTe_2/WTe_2 ⁶, Fe_3GeTe_2/WTe_2 ¹⁸, Fe_3GeTe_2/Pt ¹⁵,

Fe₃GeTe₂/Pt¹⁶, Cr₂Ge₂Te₆/Ta¹⁷, Cr₂Ge₂Te₆/Pt³³, Cr₂Ge₂Te₆/(Bi_{1-x}Sb_x)₂Te₃³⁴. Our work on CFGT/Pt device shows the first room-temperature SOT device operation without any assisted magnetic fields.

Harmonic Hall measurement is a powerful tool to study different SOT contributions and effective spin-orbit fields in magnetic heterostructures³⁵. Application of an AC current $I_{ac} = I_0 \sin \omega t$ with frequency ω modulates the SOT amplitude and induces small oscillations of M about its equilibrium direction⁴⁴. Such oscillations generate a 2nd harmonic contribution to the Hall voltage³⁶ ($V_{xy} = V_0 + V_{xy}^{1\omega} \sin \omega t + V_{xy}^{2\omega} \cos 2\omega t$), where V_{xy} depends on M_z through the AHE and the product of $M_x \times M_y$ through the planar Hall effect (PHE). The 1st harmonic term $V_{xy}^{1\omega}$ relates to the equilibrium direction of the magnetization and is independent of the modulated SOT, which was measured as an in-phase signal. The out-of-phase ($\varnothing=90^\circ$) 2nd harmonic term $V_{xy}^{2\omega}$ measures the response of the magnetization to the current-induced spin-orbit fields. The current-induced effective field ΔH can be decomposed into two components: the transverse field-like (ΔH_{FL}) and longitudinal damping-like (ΔH_{DL}) effective spin-orbit fields, which can be extracted by the following equation³⁵,

$$\Delta H_{DL(FL)} = -2 \frac{\mathbf{B}_{L(T)} + 2\xi \mathbf{B}_{T(L)}}{1 - 4\xi^2}, \quad (\text{Eq. 1})$$

where $\mathbf{B}_{L(T)} = -\frac{\partial V_{xy}^{2\omega}}{\partial H_{x(y)}}$ and $\xi = R_{PHE}/R_{AHE} \approx 1$ in CFGT/Pt heterostructure (see Supplementary Note 2 for details). The 1st harmonic term $V_{xy}^{1\omega}$ as a function of the external magnetic field H is shown in Fig. 4a. As a comparison, the out-of-plane H_z component (AHE) is presented with the in-plane field (H_x) dependent components for $\pm M_z$. Further, the 2nd harmonic term $V_{xy}^{2\omega}$ was measured vs. transverse (H_y) and longitudinal (H_x) in-plane magnetic field (Fig. 4b). By fitting the 1st and 2nd harmonic terms with Eq.1, we calculate $\Delta H_{DL}/J_{ac} = 1.9$ mT per MA/cm² and $\Delta H_{FL}/J_{ac} = 1.8$ mT per MA/cm², where J_{ac} is the current density in Pt. As the damping-like torque is attributed to the longitudinal effective spin-orbit field ΔH_{DL} , the spin-orbit torque efficiency can be calculated using expression^{37,38},

$$\xi_{DL} = T_{ini} \theta_{SH} = \frac{2e}{\hbar} \mu_0 M_s t_{CFGT}^{eff} \Delta H_{DL}/J_{ac}; \quad (\text{Eq. 2})$$

where e is the electron charge, \hbar is the reduced Plank constant, $\mu_0 M_s$ and t_{CFGT}^{eff} are the saturation magnetization (net magnetization at low field range) and the effective thickness of CFGT, respectively. Here ξ_{DL} is determined by the spin Hall angle (θ_{SH}) of Pt and the interface transparency (T_{ini}). By assuming a fully transparent interface, i.e. $T_{ini} = 1$, and spin Hall angle $\theta_{SH} = 0.12$ for Pt^{15,16,38}, we obtain the effective saturation magnetization $\mu_0 M_s \approx 12.8$ mT, which is smaller than the value of pure FM magnetic phase with the AA' crystal structure²⁵. This suggests the AFM phase has no contribution to the effective saturation magnetization at lower field range, but coexists with the FM phase, which also agrees with the SQUID magnetization and AHE results²⁴.

To further confirm the SOT contributions, we also performed large field harmonic Hall measurements. In the 1st harmonic Hall measurements with H_z field sweep (Fig. 4c), we observed the expected AFM phase transition and FM hysteresis in high and low field ranges, respectively, whereas the H_x field sweep measurement shows the FM magnetization component being pulled to the in-plane direction at around 2 T (i.e. magnetic anisotropy field, H_k), without any clear indication of the AFM transition could be detected up to 7 T. The 2nd harmonic Hall voltage signal as a function of a large in-plane field H_{ip} can help to extract the contributions from ΔH_{DL} , ΔH_{FL} and the current-induced thermal effect (Fig. 4d). Furthermore, the current dependence of the contributions from ΔH_{DL} , ΔH_{FL} and the thermal effect are plotted in Fig. 4e and Fig. 4f. We extracted $\Delta H_{DL}/J_{ac}=4.2$ mT per MA/cm² with an effective saturation magnetization $\mu_0 M_s \approx 5.9$ mT (low field) and $\Delta H_{DL}/J_{ac}=19.7$ mT per MA/cm². The current-induced Oersted field is negligible and cannot be the origin of the field-free SOT-induced magnetization switching (see details in Supplementary Note 2), while the thermal effect contribution to the harmonic Hall voltage signal $V_{xy,thermal} \propto I^2$, increasing quadratically with the current, is proportional to the M_x . Geometrically, $V_{xy,thermal} \sim M_x \times \nabla T_z$, where ∇T_z is due to the different thermal conductivity of CFGT, Pt, SiO₂/Si substrate, and air (see detailed analysis in Supplementary Note 2 and the summary of the key SOT device parameters in Supplementary Table S1). Utilizing both SOT-induced magnetic switching and 2nd harmonic Hall measurements, we can conclude that the canted magnetization in CFGT can be efficiently controlled with a switching current density of $J_{sw}=2.4 \times 10^7$ A/cm² at 300 K (see Supplementary Note 3), which is comparable to the reported values for vdW magnets at low temperatures¹⁵. Moreover, the room temperature and field-free operation of CFGT/Pt heterostructure SOT devices without any external field using a vdW magnet with coexistence of FM and AFM phases are observed for the first time (Fig. 4g), as benchmarked against the state-of-the-art.

Summary

In summary, we demonstrated the field-free and deterministic switching of the vdW magnet CFGT at room temperature, exploiting the intrinsic coexistence of non-trivial magnetic orders. Remarkably, CFGT hosts both FM and AFM properties much above room temperature, with intrinsic exchange bias and canted perpendicular ferromagnetism in a layered vdW material, which is not possible to attend in conventional systems. The detailed investigation of magnetic properties of CFGT and magnetization dynamics using SOT switching and 2nd harmonic Hall measurements of CFGT/Pt heterostructures show their relationship with observed field-free SOT behaviour. By demonstrating the feasibility of deterministic SOT-induced magnetization switching in a non-trivial vdW magnet at room temperature, our work lays the foundation for the development of novel and efficient spintronic devices based on vdW magnets, which hold

tremendous promise for next-generation non-volatile memory, logic and neuromorphic computing applications.

Methods

Fabrication of devices and electrical measurements

Device Fabrication: Single crystals of $(\text{Fe}_{0.5}\text{Co}_{0.5})_5\text{GeTe}_2$ (CFGF) were grown by chemical vapor transfer (CVT) method by HqGraphene. The AHE measurements were measured in Hall-bar devices of CFGF (20-50 nm) on SiO_2/Si substrate. The CFGF crystal was exfoliated onto the SiO_2/Si wafer, followed by electron-beam lithography (EBL) and Ar plasma etching to pattern in a Hall-bar geometry, and the Au/Ti contacts were deposited 2nd EBL step and lift-off technique. The CFGF/Pt heterostructures were prepared by exfoliating thin CFGF crystals (20-30 nm) inside an N_2 glovebox onto pre-deposited Pt(10 nm)/Ti(2 nm) layers on a SiO_2/Si substrate. The Pt layer was prepared by electron-beam evaporation onto a Si/ SiO_2 substrate with a Ti seed layer. After exfoliation, the samples were immediately transferred to an electron-beam evaporation system to deposit a 2 nm Al layer, forming an Al_2O_3 capping layer. The Hall bar and contacts were patterned using EBL and Ar ion beam etching.

Measurements: Low temperature and high magnetic field measurements of CFGF Hall bar devices were performed in the Quantum design DynaCool PPMs system with bias current in the range of 50-500 μA in the temperature range of 10-300 K and magnetic field up to 10 Tesla (T).

SOT switching and Harmonic measurements in low magnetic field range were carried out in a vacuum cryostat with a magnetic field up to 0.7 T for CFGF/Pt devices. The electronic measurements were performed using a Keithley 6221 current source, a nanovoltmeter 2182A. To monitor the longitudinal and transverse Hall resistances, Keithley 2182A nanovoltmeters were utilized. For SOT-induced magnetization switching measurements, Keithley 2182A nanovoltmeters were used to monitor the response of the Hall resistances, while a Keithley 6221 AC source was utilized with a pulse current of 100 microseconds (μs) through the device, followed by a DC read current. The harmonic measurement was performed using Lockin SR830 to measure in-phase 1st and out-of-phase 2nd harmonic voltages, respectively. The 2nd harmonic measurements in high magnetic field range were carried out in the PPMS system with an external electronic connection to Lockin SR830 to measure the 1st and 2nd harmonic voltages.

SQUID measurements: A Quantum Design superconducting quantum interference device (SQUID) was used to measure the static magnetic properties of bulk CFGF crystals. We measured the magnetic hysteresis both in in-plane ($H\parallel xy$) and out-of-plane ($H\parallel z$) magnetic fields. The bulk CFGF crystal was glued on a Si substrate to properly align the sample in the magnetic field during the measurements.

Acknowledgments

Authors acknowledge support from European Union Graphene Flagship (Core 3, No. 881603), 2D TECH VINNOVA competence center (No. 2019-00068), Swedish Research Council (VR) grant (No. 2021-04821), FLAG-ERA project 2DSOTECH (VR No. 2021-05925), KAW – Wallenberg initiative on Materials Science for a Sustainable World (WISE), Graphene Center, AoA Nano and AoA Materials program at Chalmers University of Technology. We acknowledge the help of staff at the Quantum Device Physics and Nanofabrication laboratory at Chalmers.

Data availability

The data that support the findings of this study are available from the corresponding authors at a reasonable request.

Contributions

B.Z. and S.P.D. conceived the idea and designed the experiments. B.Z. fabricated and characterized the devices with support from L.B. and R.N.. P.S. performed SQUID magnetization measurements. B.Z., S.P.D. analyzed and interpreted the experimental data, compiled the figures, and wrote the manuscript with feedback from all co-authors. S.P.D. supervised and managed the research project.

Corresponding author

Correspondence to Saroj P. Dash, saroj.dash@chalmers.se

Competing interests

The authors declare no competing interests.

References

1. Lin, X., Yang, W., Wang, K. L. & Zhao, W. Two-dimensional spintronics for low-power electronics. *Nat. Electron.* **2**, 274–283 (2019).
2. Yang, H. *et al.* Two-dimensional materials prospects for non-volatile spintronic memories. *Nature* **606**, 663–673 (2022).
3. Liu, L. *et al.* Spin-Torque Switching with the Giant Spin Hall Effect of Tantalum. *Science (80-.)*. **336**, 555–558 (2012).
4. Miron, I. M. *et al.* Perpendicular switching of a single ferromagnetic layer induced by in-plane current injection. *Nature* **476**, 189–193 (2011).
5. Manchon, A. *et al.* Current-induced spin-orbit torques in ferromagnetic and antiferromagnetic systems. *Rev. Mod. Phys.* **91**, 035004 (2019).
6. Kao, I.-H. *et al.* Deterministic switching of a perpendicularly polarized magnet using unconventional spin–orbit torques in WTe₂. *Nat. Mater.* **21**, 1029–1034 (2022).
7. Fukami, S., Zhang, C., DuttaGupta, S., Kurenkov, A. & Ohno, H. Magnetization switching by spin–orbit torque in an antiferromagnet–ferromagnet bilayer system. *Nat. Mater.* **15**, 535–541 (2016).
8. Oh, Y.-W. *et al.* Field-free switching of perpendicular magnetization through spin–orbit torque in antiferromagnet/ferromagnet/oxide structures. *Nat. Nanotechnol.* **11**, 878–884 (2016).
9. Yu, G. *et al.* Switching of perpendicular magnetization by spin–orbit torques in the absence of external magnetic fields. *Nat. Nanotechnol.* **9**, 548–554 (2014).
10. Kurebayashi, H., Garcia, J. H., Khan, S., Sinova, J. & Roche, S. Magnetism, symmetry and spin transport in van der Waals layered systems. *Nat. Rev. Phys.* **2022** *43* **4**, 150–166 (2022).
11. Huang, B. *et al.* Emergent phenomena and proximity effects in two-dimensional magnets and heterostructures. *Nat. Mater.* **2020** *1912* **19**, 1276–1289 (2020).
12. Zhao, B. *et al.* A Room-Temperature Spin-Valve with van der Waals Ferromagnet Fe₅GeTe₂/Graphene Heterostructure. *Adv. Mater.* **35**, 2209113 (2023).
13. Mak, K. F., Shan, J. & Ralph, D. C. Probing and controlling magnetic states in 2D layered magnetic materials. *Nat. Rev. Phys.* **2019** *111* **1**, 646–661 (2019).
14. Burch, K. S., Mandrus, D. & Park, J.-G. Magnetism in two-dimensional van der Waals materials. *Nature* **563**, 47–52 (2018).
15. Alghamdi, M. *et al.* Highly Efficient Spin-Orbit Torque and Switching of Layered Ferromagnet Fe₃GeTe₂. *Nano Lett.* **19**, 4400–4405 (2019).
16. Wang, X. *et al.* Current-driven magnetization switching in a van der Waals ferromagnet Fe₃GeTe₂. *Sci. Adv.* **5**, eaaw8904 (2019).
17. Ostwal, V., Shen, T. & Appenzeller, J. Efficient Spin-Orbit Torque Switching of the Semiconducting

- Van Der Waals Ferromagnet Cr₂Ge₂Te₆. *Adv. Mater.* **32**, 1906021 (2020).
18. Shin, I. *et al.* Spin–Orbit Torque Switching in an All-Van der Waals Heterostructure. *Adv. Mater.* **34**, 2101730 (2022).
 19. Liu, L., Lee, O. J., Gudmundsen, T. J., Ralph, D. C. & Buhrman, R. A. Current-Induced Switching of Perpendicularly Magnetized Magnetic Layers Using Spin Torque from the Spin Hall Effect. *Phys. Rev. Lett.* **109**, 096602 (2012).
 20. MacNeill, D. *et al.* Control of spin–orbit torques through crystal symmetry in WTe₂/ferromagnet bilayers. *Nat. Phys.* **13**, 300–305 (2017).
 21. Liu, L. *et al.* Current-induced magnetization switching in all-oxide heterostructures. *Nat. Nanotechnol.* **14**, 939–944 (2019).
 22. Tian, C. *et al.* Tunable magnetic properties in van der Waals crystals (Fe_{1-x}Co_x)₅GeTe₂. *Appl. Phys. Lett.* **116**, 202402 (2020).
 23. Zhang, H. *et al.* A room temperature polar magnetic metal. *Phys. Rev. Mater.* **6**, 044403 (2022).
 24. May, A. F., Du, M.-H., Cooper, V. R. & McGuire, M. A. Tuning magnetic order in the van der Waals metal Fe₅GeTe₂ by cobalt substitution. *Phys. Rev. Mater.* **4**, 074008 (2020).
 25. Zhang, H. *et al.* Room-temperature skyrmion lattice in a layered magnet (Fe_{0.5}Co_{0.5})₅GeTe₂. *Sci. Adv.* **8**, (2022).
 26. Jiang, S., Shan, J. & Mak, K. F. Electric-field switching of two-dimensional van der Waals magnets. *Nat. Mater.* **17**, 406–410 (2018).
 27. Telford, E. J. *et al.* Coupling between magnetic order and charge transport in a two-dimensional magnetic semiconductor. *Nat. Mater.* **21**, 754–760 (2022).
 28. Telford, E. J. *et al.* Layered Antiferromagnetism Induces Large Negative Magnetoresistance in the van der Waals Semiconductor CrSBr. *Adv. Mater.* **32**, 2003240 (2020).
 29. Stamps, R. L. Mechanisms for exchange bias. *J. Phys. D: Appl. Phys.* **33**, R247–R268 (2000).
 30. Zhang, S., Levy, P. M. & Fert, A. Mechanisms of Spin-Polarized Current-Driven Magnetization Switching. *Phys. Rev. Lett.* **88**, 236601 (2002).
 31. Krishnaswamy, G. K. *et al.* Time-Dependent Multistate Switching of Topological Antiferromagnetic Order in Mn₃Sn. *Phys. Rev. Appl.* **18**, 024064 (2022).
 32. Pal, B. *et al.* Setting of the magnetic structure of chiral kagome antiferromagnets by a seeded spin-orbit torque. *Sci. Adv.* **8**, 5930 (2022).
 33. Gupta, V. *et al.* Manipulation of the van der Waals Magnet Cr₂Ge₂Te₆ by Spin-Orbit Torques. *Nano Lett.* **20**, 7482–7488 (2020).
 34. Mogi, M. *et al.* Current-induced switching of proximity-induced ferromagnetic surface states in a topological insulator. *Nat. Commun.* **12**, 1404 (2021).
 35. Hayashi, M., Kim, J., Yamanouchi, M. & Ohno, H. Quantitative characterization of the spin-orbit torque using harmonic Hall voltage measurements. *Phys. Rev. B* **89**, 144425 (2014).
 36. Avci, C. O. *et al.* Interplay of spin-orbit torque and thermoelectric effects in ferromagnet/normal-metal bilayers. *Phys. Rev. B* **90**, 224427 (2014).
 37. Pai, C.-F., Ou, Y., Vilela-Leão, L. H., Ralph, D. C. & Buhrman, R. A. Dependence of the efficiency of spin Hall torque on the transparency of Pt/ferromagnetic layer interfaces. *Phys. Rev. B* **92**, 064426 (2015).
 38. Nguyen, M.-H., Ralph, D. C. & Buhrman, R. A. Spin Torque Study of the Spin Hall Conductivity and Spin Diffusion Length in Platinum Thin Films with Varying Resistivity. *Phys. Rev. Lett.* **116**, 126601 (2016).